Observation of Temperature-Dependent Capture Cross-Section for Main Deep-Levels in β-Ga_2O_3

A.A. Vasilev [1], A.I. Kochkova [1], A.Y. Polyakov [1], A.A. Romanov [1], N.R. Matros [1], L.A. Alexanyan [1], I.V. Shchemerov [1] and S.J. Pearton [2]

1) National University of Science and Technology MISIS, Leninsky pr. 4, Moscow 119049, Russia
2) Department of Materials Science and Engineering, University of Florida, Gainesville, Florida 32611, USA

Abstract:

Direct observation of capture cross-section is challenging due to the need of extremely short filling pulses in the two-gate Deep-Level Transient Spectroscopy (DLTS). Simple estimation of cross-section can be done from DLTS and Admittance Spectroscopy (AS) data, but it is not feasible to distinguish temperature dependence of pre-exponential and exponential parts of the emission rate equation with sufficient precision conducting a single experiment. This paper presents experimental data of deep-levels in β-Ga_2O_3 that has been gathered by our group since 2017. Based on the gathered data we propose a derivation of apparent activation energy (E_a^m) and capture cross-section (σ_n^m) assuming temperature dependent capture via multiphonon emission model, which resulted in strong correlation between E_a^m and σ_n^m according to Meyer-Neldel rule, which allowed us to estimate low- and high-temperature capture coefficients C_0 and C_1 as well as capture barrier E_b. It also has been shown that without considering the temperature dependence of capture cross-section, the experimental values of σ_n are overestimated by 1-3 orders of magnitude. A careful consideration of the data also allows to be more certain identifying deep-levels by their "fingerprints" (E_a and σ_n) considering two additional parameters (E_{MN} and σ_{00}) and to verify the density functional theory (DFT) computation of deep-level recombination properties.

Keywords: semiconductors, DLTS, defects, deep-levels, capture coefficient, recombination, β-Ga_2O_3

1. Introduction

In recent years, Ga_2O has been actively investigated by numerous research groups due to its promising potential for power electronics and solar-blind UV detectors.[1,2] To advance the application of gallium oxide devices, detailed studies have been conducted on crystal growth,[1,3,4] epitaxial film growth,[1] intentional doping, and electrically active defects.[3] Our emphasis has been focused on the deep-level defects investigation by capacitance spectroscopy, mainly Deep-Level Transient Spectroscopy (DLTS)[5] and Admittance Spectroscopy (AS).[6,7] These two techniques are widely used for characterizing electrically active defects by evaluating their concentration (N_t), thermal activation energy (E_a), and electron capture cross section (σ_n).

These parameters are obtained from electron detrapping-kinetics characterized by the emission rate $e_n(T)$ dependence on temperature T, as given by:[5]

$$e_n(T) = \sigma_n \gamma T^2 \exp\left(-\frac{E_a}{kT}\right) \tag{1}$$

where $\gamma = 4\sqrt{6} \cdot k^2\, \pi^{3/2} h^{-3} m^*$, m^* is an effective mass, T is the temperature, k the Boltzmann constant. Here σ_n is assumed to be independent of temperature.

The kinetics of many thermally activated processes in chemistry and physics, including the emission rate of carriers from deep levels, are usually calculated from so called Arrhenius plots, which allow to extract the pre-exponential factor and activation energy as the temperature independent parameters for the sake of mathematical treatment simplification. This approach works well for simple estimation kinetics phenomena, however, if one is lacking knowledge of exact temperature dependence of pre-exponential factor and activation energy, it is not possible to reduce it to Arrhenius equation term by term and, therefore, the kinetics cannot be characterized with high precision. Furthermore, a capture cross-section and activation energy cannot be determined accurately.

1.1 **Meyer-Neldel rule in semiconductors**

In terms of semiconductor physics, this problem was faced by W. Meyer and H. Neldel in 1937 when they proposed empirical relationship given in equation (2) of the temperature dependence of pre-exponential factor for thermally activated conductivity.[8] This empirical law for the pre-exponential factor temperature dependence for thermally activated conductivity was presented and is now called Meyer-Neldel rule (MNR).

$$\sigma_0 = \sigma_{00} \exp\left(-\frac{E_a}{E_{MN}}\right) \tag{2}$$

Various research groups confirmed this rule for carrier emission kinetics in A3B5 compounds,[9,10] ZnO and other semiconductors.[11,12] The most reasonable physical explanation of the MNR in terms of emission rate is based on considering the total change in Gibbs energy with entropy part as attributed to vibrational entropy ΔS_{vib}. It has been concluded that vibrational entropy (estimated as rearrangement entropy of n interacting phonons of N total phonons in interaction volume) $\Delta S_{\mathrm{vib}}/k_B = E_a/E_{MN} \cong n \ln(N/n)$ could not explain extremely small values of σ_{00} which are ~10^{-23} cm^2, and that without accumulation of a significant amount of data, it is not clear whether new ideas on this issue will be proposed.[11]

From the theoretical side, Alkauskas et. al. in 2014 developed[13] a theory on computing nonradiative capture cross-section for deep-level transitions occurring via multiphonon emission, which gives insights on defect recombinational properties at different temperatures and allows to identify defects from experimental data.

This current paper reveals new aspects of experimental deep-level parameters determination, provides results to verify such DFT defects computations, and demonstrates new data on capture coefficients for the main electron traps in β-Ga_2O_3.

2. Sampling

This analysis is based on DLTS and Admittance Spectroscopy data that has been gathered since 2017 for deep-levels in a wide range of β-Ga_2O_3 samples. The studied samples of β-Ga_2O_3 were cut from various types of wafers purchased from Tamura/Novel Crystals, Inc., Tokyo, Japan: β-Ga_2O_3 (-201) and (010) oriented edge defined film-fed grown (EFG) wafers doped with Sn, unintentionally doped EFG (-201) wafer, (010) oriented EFG wafers doped with Fe and (001) orientated unintentionally doped halide vapor phase epitaxy (HVPE) grown layers on bulk n^+-EFG substrates doped with Sn.[14] Different sets of treatments were employed to understand the presence and origin of electrically active deep levels in β-Ga_2O_3. A detailed description of the experiments and results along with the depiction of the deep-levels spectra could be found in our previous works.[15–21]

The sampling contains 1242 uncategorized data entities each corresponding to a single measurement of activation energy (E_a^m) and capture cross-section (σ_n^m) from Arrhenius plot in $\ln(e_n T^{-2})$ vs $1/T$ axes. The peak temperature (T_{peak}) is taken at the smallest window in the measurement and used only to improve quality of deep-level data clustering.

Up to now, a large number of groups have already done a significant work in the field of theoretical and experimental identification of electrically active defects in gallium oxide. Let us briefly describe the results of deep-levels characterization that are taken as reference data in this analysis.

Center E1 (with E_a found in range (0,45÷0,65) eV, and σ_n found in range (0.3÷7)·10^{-13} cm^2) has been introduced by H-plasma treatment,[19] proton irradiation,[18,21] and ampoule annealing in H_2.[15,22] It has been observed that the E1 is a donor, and according to the theoretical models, a possible configuration is the complex of H with shallow donors Si or Sn.[15]

The center E2 (E_a=(0,74÷0,82) eV, σ_n=(0.6÷23)·10^{-15} cm^2) is often detected in EFG, HVPE grown samples and assigned to Fe acceptors.[23–32] The E2* centers (E_a=(0,75÷0,78) eV, σ_n=(2÷7)·10^{-14} cm^2) typically have been observed after radiation or implantation and demonstrates a linear increase with irradiation exposure.[21] This implies the possible origin of E2 , which is a complex of intrinsic point defects of gallium and oxygen vacancies.[32]

For the E3 (E_a=1.05 eV, σ_n=4.1·10^{-13} cm^2) level detected in unintentionally doped EFG-grown β-Ga_2O_3, it has been suggested that the possible nature of the center is a deep donor related to Ti.[33] However, a defect with a similar E_a and σ_n tends to increase in concentration after irradiation with high-energy particles (neutrons and protons) and Ar plasma treatment.[21] So, the issue with these two interpretations could be the same as for E2 and E2* at early stages of β-Ga_2O_3 research.[32]

The E8 (E_a=0,28 eV, σ_n=6·10^{-18} cm^2) center is an intrinsic point defect or complex detected after irradiations and treatment with Ar and H plasma.[21]

2.1 **Deep-level clustering**

Data clustering was performed using a Gaussian Mixture model with Variational inference algorithm.[34] This method assumes all data can be represented by finite mixture of Gaussian distributions with unknown parameters which are determined from a variational lower boundary. The above procedure reduced the total data entities from 1242 to 1033, excluding dropouts, and produced 6 clusters assigned as main deep-levels E2*, E4, E8, E1, E2 and E3. Results of data clustering can be seen in the pairwise plot in Figure 1, where normalized distributions of σ_n^m, E_a^m and T_{peak} for each trap are presented on the main diagonal plots and pairs of parameters plotted pairwise on off-diagonal plots.

Variances and mean values of σ_n^m, E_a^m and T_{peak} for each deep-level can be determined from the data presented in Figures 1a, 1e and 1i. The vertical alignment of clusters on Figures 1c, and 1f demonstrates no correlation of σ_n^m and E_a^m with T_{peak} (since σ_n^m and E_a^m are computed from Arrhenius plots in temperature ranges higher than T_{peak} variance) but there is strong correlation of σ_n^m with E_a^m on Figure 1b. This relationship will be used further for equation (2) fit and results analysis.

3. Derivations

Typically, the most straightforward and accurate way to determine capture cross-section is through direct observation of capture kinetics, but this method necessitates the usage of extremely short pulsing times even for materials with low doping levels in the two-gate DLTS[35] ($\tau_p{}^{-1} = C_n \cdot n \approx 10^{-9} \cdot 10^{15} = 1$ MHz). More simple ways are to calculate the capture cross-section from standard DLTS and AS approaches,[5–7] but these techniques are not suitable for precise capture cross-section measurements, especially with the assumption of its strong temperature dependance. Emission rates can be measured by implementing long and short windows for DLTS to compute the low- and high-temperature cross-section from Arrhenius plots, but in this case, it is not feasible to separate the temperature dependence of pre-exponential and exponential parts with sufficient precision conducting a single experiment.

The following sections will reveal a treatment of this issue which allows to extract activation energy (E_a), low- and high-temperature capture coefficients (C_0, C_1), and capture barrier (E_b) of the deep-level through detailed DLTS and AS data analysis.

3.1 Vibrational entropy

The entropy term, as mentioned in the introduction, was proposed to explain the observed correlation of E_a and σ_n for other semiconductor materials. In addition, its appearance in Gibbs

free energy ($-\Delta G/kT = -\Delta H/kT + \Delta S/k$) fits well with temperature independent behavior described by equation (2), but the vibrational entropy is relatively small $\Delta S_{\text{vib}}/k = \pm(1.5 \div 3)$[36,37] when atomic rearrangements around defect are neglected.

3.2 **Carrier capture by multiphonon emission**

The attempt to consider coupling with local mode Q can be done with the given temperature dependence of carrier capture via multiphonon emission. The capture coefficient can be written in its low-temperature form (3),[38] with p and S defined from configurational diagram (Fig. 2)

$$C_n \propto (\bar{n}+1)^p \frac{S^p}{p!} \exp\left(-2S\left(\bar{n}+\frac{1}{2}\right)\right) \tag{3}$$

The expression (3) can be approximated at low and high temperatures with the equation (4):[13,38]

$$C_n(T) \approx C_0 + C_1 \exp\left(-\frac{E_b}{kT}\right) \tag{4}$$

And then capture cross-section by definition will be:

$$\sigma_n(T) = C_n(T)/\langle v_{th}\rangle \tag{5}$$

where $\langle v_{th}\rangle = \sqrt{3kT/m^*}$ – average thermal velocity. Thus, the temperature dependence of emission rates for carriers trapped at deep-level ($E_a = E_k(0) - E_d(Q_d)$) will be:

$$e_n = \sigma_n(T) \cdot \gamma T^2 \exp\left(-\frac{E_a}{kT}\right) \tag{6}$$

Since the emission rate data from DLTS/AS experiment is treated with Arrhenius plot, we need to analytically keep temperature dependence of (6) until we will be ready to understand nature of observed E_a^m and σ_n^m correlation (Fig. 1b) and then simplify resulted expression in order to estimate coefficients of equation (4). Arrhenius plot (Fig. 3a) in $\ln(e_n T^{-2})$ vs $1/T$ axes after collecting results from equations (4), (5) and (6) will be:

$$\ln(e_n T^{-2}) = -\ln\langle v_{th}\rangle + \ln\gamma + \ln\left(C_0 + C_1 \exp\left(-\frac{E_b}{kT}\right)\right) - \frac{E_a}{kT} \tag{7}$$

Therefore, apparent activation energy is computed from the slope of a tangent line at temperature T in $\ln(e_n T^{-2})$ vs $1/T$ axes. This slope as a function of temperature will be:

$$\text{slope}(T) = \frac{d}{d(1/T)} \ln(e_n T^{-2}) = \frac{1}{2} T - \frac{E_b/k \cdot C_1}{C_0 e^{\frac{E_b}{kT}} + C_1} - \frac{E_a}{k} \tag{8}$$

And corresponding intercept of a tangent line ($\text{intercept}(x) = f(x) - x \cdot f'(x)$) at temperature T, from which apparent capture cross-section is computed in $\ln(e_n T^{-2})$ vs $1/T$ axes will be:

$$\text{intercept}(T) = -\ln\langle v_{th}\rangle + \ln\gamma + \ln\left(C_0 + C_1 \exp\left(-\frac{E_b}{kT}\right)\right) - \frac{E_a}{kT} - \frac{1}{T} \cdot \text{slope}(T) \tag{9}$$

Eventually, measured E_a^m and σ_n^m from slope and intercept at some temperature T will be:

$$E_a^m = -\text{slope}(T) \cdot k, \tag{10}$$

$$\sigma_n^m = \frac{\exp(\text{intercept}(T))}{\gamma}. \tag{11}$$

It can be clearly seen from (8) and (10) that E_a^m appears to be step-like function (Fig. 3b) of T, with low- and high-temperature plateaus that are roughly E_a and $E_a + E_b$, with shift due to the presence of $-kT/2$ in E_a^m. More precise values for lower and upper boundaries are $(E_a - \Delta)$ and $(E_a + E_b - \Delta)$ where shift value Δ is $\Delta = -E_b(\ln(C_1/C_0) - 2)/(2\ln^2(C_1/C_0))$. The same temperature behavior of $\ln(\sigma_n^m)$ is presented on Fig. 3c with the lower and upper boundaries at the same temperatures as E_a^m.

In order to reproduce results from Fig 1b, the derivative of $\ln(\sigma_n^m)$ with respect to E_a^m will be:

$$\frac{d(\ln(\sigma_n^m))}{dE_a^m} = \frac{(\partial \ln(\sigma_n^m)/\partial T) \cdot dT}{(\partial E_a^m/\partial T) \cdot dT} = \frac{1}{kT} \tag{12}$$

Summing up the intermediate results, (10) and (11) implies that E_a^m and $\ln(\sigma_n^m)$ correlates through the temperature at which DLTS/AS can be performed, but experimentally we are limited in the analysis for the same reason elaborated in section 2.1 – data points from DLTS/AS data taken in broad temperature interval (around $\Delta T \approx 50\text{K}$ for E2 trap) when noticeable changes in E_a^m or $\ln(\sigma_n^m)$ are happening in narrow temperature range. This narrow temperature range appears form data linearity in Fig 1b implying by (12) ($1/kT$ should be constant or vary slow to give linearity in Fig. 1b).

The gathered data for E2 trap (Fig. 3b,c) shows that changes in $\ln(\sigma_n^m)$ occur in a narrow temperature region near some temperature T_m so almost linear data in $\ln(\sigma_n^m)$ vs E_a^m axes will be observed. To estimate T_m it can be assumed that $E_a^m(T_m)$ and $\sigma_n^m(T_m)$ corresponds to the middle of the step of (10) and (11) leading to same result for T_m (Fig. 3b,c):

$$E_a^m(T_m) = E_a + \frac{E_b}{2} \Longrightarrow T_m = \frac{E_b}{k\ln(C_1/C_0)} \tag{13}$$

$$\frac{C_1}{C_0}\exp\left(-\frac{E_b}{kT_m}\right) = 1 \Longrightarrow T_m = \frac{E_b}{k\ln(C_1/C_0)} \tag{14}$$

Since E_a^m and $\ln(\sigma_n^m)$ data shows no correlation to T_{peak} due to experiment limitations, and the biggest changes in measured parameters appears around T_m, we can expand $E_a^m(T)$ and $\ln\sigma_n^m(T)$ near T_m, excluding temperature from equations and establishing functional dependence in form $\ln(\sigma_n^m) = f(E_a^m)$.

So, expanding E_a^m at T_m up to the linear term:

$$E_a^m(T)\,\big|_{T_m} \approx E_a^m(T_m) + \frac{dE_a^m}{dT}\,\big|_{T_m}(T - T_m) + O(T^2)$$

$$= E_a + E_b\left(\frac{1}{2} - \frac{\ln(C_1/C_0)}{4}\right) + kT\left(\frac{\ln^2(C_1/C_0)}{4} - \frac{1}{2}\right) \tag{15}$$

And for $\ln(\sigma_n^m)$ at T_m:

$$\ln\sigma_n^m(T)\,\big|_{T_m} \approx \ln\sigma_n^m(T_m) + \frac{d\ln\sigma_n^m}{dT}\,\big|_{T_m}(T - T_m) + O(T^2)$$

$$= \ln(2C_0) - \frac{1}{4}\left(\ln^2\left(\frac{C_1}{C_0}\right) - 2\ln\left(\frac{C_1}{C_0}\right)\right) - \frac{1}{2}\ln\left(\frac{3E_b}{m^*\ln(C_1/C_0)}\right) \tag{16}$$

$$+ \frac{kT}{E_b}\left(\frac{\ln^3(C_1/C_0)}{4} - \frac{\ln(C_1/C_0)}{2}\right)$$

Expressing and equating T from (15) and (16) brings us to $\ln(\sigma_n^m) = f(E_a^m)$ near T_m, which allows to extract deep-level parameters from fitting the resultant expression for red line in Fig. 3:

$$f(x) = \ln(2C_0) - \frac{E_a}{E_b}\ln\left(\frac{C_1}{C_0}\right) - \frac{1}{2}\ln\left(\frac{3E_b}{m^*\ln(C_1/C_0)}\right) + x\frac{\ln(C_1/C_0)}{E_b} \tag{17}$$

From $f(x = 0)$ condition low-temperature capture coefficient C_0 can be estimated with experimentally known σ_{00}:

$$\sigma_{00} = \frac{2C_0}{\sqrt{\frac{3kT_m}{m^*}}}\exp\left(-\frac{E_a}{kT_m}\right) \tag{18}$$

3.3 Model fitting

To find all 4 (E_a, E_b, C_0, C_1) model parameters from experimental data it is needed to impose two more restrictions besides (13) and (18).

Assuming that enough data from many different time windows has been gathered and, therefore, the mean values of this data are represented by $E_a^m(T_m)$ and ln $\sigma_n^m(T_m)$, the complete system of equations can we written:

$$\begin{cases} E_a + \dfrac{E_b}{2} \approx \mathrm{mean}(E_a^m), & \text{(i)} \\ \log_{10}\left(\dfrac{2\sqrt{C_1 C_0}}{\sqrt{3kT_m/m^*}} \exp(-1/2)\right) \approx \mathrm{mean}\left(\log_{10}(\sigma_n^m)\right), & \text{(ii)} \\ \dfrac{E_b}{k\ln(C_1/C_0)} = T_m, & \text{(iii)} \\ \log_{10}\left(\dfrac{2C_0}{\sqrt{3kT_m/m^*}} \exp\left(-\dfrac{E_a}{kT_m}\right)\right) = \log_{10}(\sigma_{00}). & \text{(iv)} \end{cases} \quad (19)$$

This system can’t be solved analytically, so it might be suggested to use the numerical approach of finding the solution by minimizing the following function:

$$F = \sum_{i=1}^{4} f_i - f_i^{\mathrm{RHS}} \quad (20)$$

And corresponding solution will be:

$$E_a, E_b, C_0, C_1\colon \quad \min_{E_a, E_b, C_0, C_1} \{\|F\|_2^2\} \leq 10^{-5} \quad (21)$$

4. Results

Computed $E_{MN} = kT_m$ and σ_{00} for deep-levels E2, E2*, E1, E8 and E3 (E4 is omitted here due to the lack of extensive collected data) in β-Ga_2O_3 are presented in Fig. 4. This data is then used for solving Eq. (21) to provide the right-hand side for equation (iii) and (iv) of (19).

The distributions of gathered E_a^m and σ_n^m are represented in box-plots on Fig. 5. Boxes on Figure 5 represent $\mathrm{mean}(E_a^m)$ and $\mathrm{mean}\left(\log_{10}(\sigma_n^m)\right)$ at temperature T_m and used as right-hand side of equations (i) and (ii) of (19). Solutions of (21) for each trap are presented in Table 1 and plotted in Figure 6.

In comparison with Fig. 5, activation energies and capture cross-sections obtained in experiments are overestimated due to interplay of the temperature dependence of capture cross-section and the thermal emission terms, and, in this case, the previously measured values of capture cross-section (around T_{peak}) are 1-3 orders of magnitude higher than obtained with suggested model.

Approaching the same problem from theoretical side of the issue, similar results were obtained by Wickramaratne et al. [39] In their paper, computed temperature dependent capture cross-section via multiphonon emission mechanism was inserted into DLTS formalism, and it appeared to shift apparent activation energy obtained from Arrhenius plot to higher values at higher temperatures. Nevertheless, the study[39] was not supported by any experimental data, unlike the present paper, which is possibly the first experimental observation on this matter.

5. Summary and Conclusions

In this paper we have considered that the carrier emission rate from main deep-levels in β-Ga_2O_3 follow the MN-rule and it has been shown that the capture cross section in multiphonon emission model explains the observed E_a^m and σ_n^m shift.

We have applied the theory to the main deep-level centers in β-Ga_2O_3 and accurately calculated all parameters (Table 1), including activation energy E_a, barrier height for carrier capture E_b, as well as low- and high-temperature capture coefficients C_0 and C_1.

This suggests using of E_{MN} and σ_{00} as two additional parameters to identify defects, employing of C_0, C_1 and E_b to estimate capture coefficient with more detailed and advanced approach, and to verify DFT results on recombinational properties of deep levels.

Acknowledgments

The research at NUST MISIS was funded by Ministry of Science and Higher Education of the Russian Federation grant number 075-15-2022-1113. The work at UF was performed as part of Interaction of Ionizing Radiation with Matter University Research Alliance (IIRM-URA), sponsored by the Department of the Defence, Defence Threat Reduction Agency under award HDTRA1-20-2-0002. The content of the information does not necessarily reflect the position or the policy of the federal government, and no official endorsement should be inferred.

Data availability statement

The data that support the findings of this study are available from the A.A. Vasilev, upon reasonable request.

References

[1] Masataka Higashiwaki, and Shizuo Fujita, *Gallium Oxide* (Springer International Publishing, Cham, 2020).

[2] Fan Ren, and Stephen J Pearton, *Wide Bandgap Semiconductor-Based Electronics* (IOP Publishing, 2020).

[3] E. Farzana, and J.S. Speck, "Introduction," in *Ultrawide Bandgap β-Ga2O3 Semiconductor*, (AIP Publishing, 2023), pp. 1–34.

[4] N. Xia, Y. Liu, D. Wu, L. Li, K. Ma, J. Wang, H. Zhang, and D. Yang, "β-Ga2O3 bulk single crystals grown by a casting method," J Alloys Compd **935**, 168036 (2023).

[5] D. V. Lang, "Deep-level transient spectroscopy: A new method to characterize traps in semiconductors," J Appl Phys **45**(7), 3023–3032 (1974).

[6] C.T. Sah, L. Forbes, L.L. Rosier, and A.F. Tasch, "Thermal and optical emission and capture rates and cross sections of electrons and holes at imperfection centers in semiconductors from photo and dark junction current and capacitance experiments," Solid State Electron **13**(6), 759–788 (1970).

[7] G. Vincent, D. Bois, and P. Pinard, "Conductance and capacitance studies in GaP Schottky barriers," J Appl Phys **46**(12), 5173–5178 (1975).

[8] W. Meyer, and H. Neldel, "Relation between the energy constant and the quantity constant in the conductivity–temperature formula of oxide semiconductors," Z. Tech. Phys. **12**(588), (1937).

[9] R.S. Crandall, "Meyer-Neldel Rule in Deep-Level-Transient-Spectroscopy and its Ramifications," MRS Proceedings **763**, B2.5 (2003).

[10] R.S. Crandall, "Analysis of Emission Rate Measurements in a Material Showing a Meyer-Neldel- Rule," MRS Proceedings **799**, Z1.6 (2003).

[11] H. Schmidt, M. Wiebe, B. Dittes, and M. Grundmann, "Meyer-Neldel rule in ZnO," Appl Phys Lett **91**(23), (2007).

[12] J.A.M. AbuShama, S.W. Johnston, R.S. Crandall, and R. Noufi, "Meyer-Neldel rule and the influence of entropy on capture cross-section determination in Cu(In,Ga)Se2," Appl Phys Lett **87**(12), (2005).

[13] A. Alkauskas, Q. Yan, and C.G. Van de Walle, "First-principles theory of nonradiative carrier capture via multiphonon emission," Phys Rev B **90**(7), 075202 (2014).

[14] "Tamura Corp. b-Ga2O3 Substrates," (n.d.).

[15] A.Y. Polyakov, A.I. Kochkova, A. Langørgen, L. Vines, A. Vasilev, I. V. Shchemerov, A.A. Romanov, and S.J. Pearton, "On the possible nature of deep centers in Ga2O3," Journal of Vacuum Science & Technology A **41**(2), (2023).

[16] A.Y. Polyakov, I.-H. Lee, N.B. Smirnov, E.B. Yakimov, I. V. Shchemerov, A. V. Chernykh, A.I. Kochkova, A.A. Vasilev, P.H. Carey, F. Ren, D.J. Smith, and S.J. Pearton, “Defects at the surface of β-Ga2O3 produced by Ar plasma exposure,” APL Mater **7**(6), (2019).

[17] A.Y. Polyakov, N.B. Smirnov, I. V. Schemerov, A. V. Chernykh, E.B. Yakimov, A.I. Kochkova, A.N. Tereshchenko, and S.J. Pearton, “Electrical Properties, Deep Levels and Luminescence Related to Fe in Bulk Semi-Insulating β-Ga_2O_3 Doped with Fe,” ECS Journal of Solid State Science and Technology **8**(7), Q3091–Q3096 (2019).

[18] J. Kim, S.J. Pearton, C. Fares, J. Yang, F. Ren, S. Kim, and A.Y. Polyakov, “Radiation damage effects in Ga_2O_3 materials and devices,” J Mater Chem C Mater **7**(1), 10–24 (2019).

[19] A.Y. Polyakov, E.B. Yakimov, V.I. Nikolaev, A.I. Pechnikov, A. V. Miakonkikh, A. Azarov, I.-H. Lee, A.A. Vasilev, A.I. Kochkova, I. V. Shchemerov, A. Kuznetsov, and S.J. Pearton, “Impact of Hydrogen Plasma on Electrical Properties and Deep Trap Spectra in Ga2O3 Polymorphs,” Crystals (Basel) **13**(9), 1400 (2023).

[20] A.Y. Polyakov, N.B. Smirnov, I. V. Shchemerov, E.B. Yakimov, J. Yang, F. Ren, G. Yang, J. Kim, A. Kuramata, and S.J. Pearton, “Point defect induced degradation of electrical properties of Ga2O3 by 10 MeV proton damage,” Appl Phys Lett **112**(3), (2018).

[21] A.Y. Polyakov, V.I. Nikolaev, E.B. Yakimov, F. Ren, S.J. Pearton, and J. Kim, “Deep level defect states in β-, α-, and *ε* -Ga2O3 crystals and films: Impact on device performance,” Journal of Vacuum Science & Technology A **40**(2), (2022).

[22] A. Langørgen, C. Zimmermann, Y. Kalmann Frodason, E. Førdestrøm Verhoeven, P. Michael Weiser, R. Michael Karsthof, J. Basile Varley, and L. Vines, “Influence of heat treatments in H2 and Ar on the *E* 1 center in *β* -Ga2O3,” J Appl Phys **131**(11), (2022).

[23] C. Zimmermann, Y. Kalmann Frodason, V. Rønning, J.B. Varley, and L. Vines, “Combining steady-state photo-capacitance spectra with first-principles calculations: the case of Fe and Ti in β-Ga_2O_3,” New J Phys **22**(6), 063033 (2020).

[24] M.E. Ingebrigtsen, A.Yu. Kuznetsov, B.G. Svensson, G. Alfieri, A. Mihaila, U. Badstübner, A. Perron, L. Vines, and J.B. Varley, “Impact of proton irradiation on conductivity and deep level defects in β-Ga2O3,” APL Mater **7**(2), (2019).

[25] M.E. Ingebrigtsen, L. Vines, G. Alfieri, A. Mihaila, U. Badstübner, B.G. Svensson, and A. Kuznetsov, “Bulk β-Ga₂O₃ with (010) and (201) Surface Orientation: Schottky Contacts and Point Defects,” Materials Science Forum **897**, 755–758 (2017).

[26] E. Farzana, M.F. Chaiken, T.E. Blue, A.R. Arehart, and S.A. Ringel, “Impact of deep level defects induced by high energy neutron radiation in β-Ga2O3,” APL Mater **7**(2), (2019).

[27] Z. Zhang, E. Farzana, A.R. Arehart, and S.A. Ringel, “Deep level defects throughout the bandgap of (010) β-Ga2O3 detected by optically and thermally stimulated defect spectroscopy,” Appl Phys Lett **108**(5), (2016).

[28] Y.-Y. Lin, A.T. Neal, S. Mou, and J. V. Li, "Study of defects in β-Ga2O3 by isothermal capacitance transient spectroscopy," Journal of Vacuum Science & Technology B, Nanotechnology and Microelectronics: Materials, Processing, Measurement, and Phenomena **37**(4), (2019).

[29] H. Ghadi, J.F. McGlone, E. Cornuelle, Z. Feng, Y. Zhang, L. Meng, H. Zhao, A.R. Arehart, and S.A. Ringel, "Deep level defects in low-pressure chemical vapor deposition grown (010) β-Ga2O3," APL Mater **10**(10), (2022).

[30] J.F. Mcglone, Z. Xia, Y. Zhang, C. Joishi, S. Lodha, S. Rajan, S.A. Ringel, and A.R. Arehart, "Trapping Effects in Si -Doped -Ga $_2$ O $_3$ MESFETs on an Fe-Doped -Ga $_2$ O $_3$ Substrate," IEEE Electron Device Letters **39**(7), 1042–1045 (2018).

[31] K. Irmscher, Z. Galazka, M. Pietsch, R. Uecker, and R. Fornari, "Electrical properties of β -Ga2O3 single crystals grown by the Czochralski method," J Appl Phys **110**(6), (2011).

[32] M.E. Ingebrigtsen, J.B. Varley, A.Yu. Kuznetsov, B.G. Svensson, G. Alfieri, A. Mihaila, U. Badstübner, and L. Vines, "Iron and intrinsic deep level states in Ga2O3," Appl Phys Lett **112**(4), (2018).

[33] C. Zimmermann, Y.K. Frodason, A.W. Barnard, J.B. Varley, K. Irmscher, Z. Galazka, A. Karjalainen, W.E. Meyer, F.D. Auret, and L. Vines, "Ti- and Fe-related charge transition levels in β−Ga2O3," Appl Phys Lett **116**(7), (2020).

[34]"scikit-learn. Variational Bayesian Gaussian Mixture," (n.d.).

[35] D. Pons, "Accurate determination of the free carrier capture kinetics of deep traps by space-charge methods," J Appl Phys **55**(10), 3644–3657 (1984).

[36] M. Lannoo, and J. Bourgoin, "Vibrational Properties and Entropy," (1981), pp. 155–190.

[37] C. Lee, N.D. Rock, A. Islam, M.A. Scarpulla, and E. Ertekin, "Electron–phonon effects and temperature-dependence of the electronic structure of monoclinic β -Ga2O3," APL Mater **11**(1), (2023).

[38] J. Bourgoin, and M. Lannoo, "Carrier Emission and Recombination," (1983), pp. 154–204.

[39] D. Wickramaratne, C.E. Dreyer, B. Monserrat, J.-X. Shen, J.L. Lyons, A. Alkauskas, and C.G. Van de Walle, "Defect identification based on first-principles calculations for deep level transient spectroscopy," Appl Phys Lett **113**(19), (2018).

Table 1. Results of model fitting for main deep-levels in β-Ga_2O_3

Trap	E_a (eV)	E_b (eV)	C_0 (cm^3/s)	C_1 (cm^3/s)
E2	0.68	0.21	7.0×10^{-10}	1.4×10^{-6}
E2*	0.61	0.21	1.3×10^{-9}	2.6×10^{-6}
E1	0.52	0.17	1.3×10^{-8}	3.1×10^{-5}
E8	0.23	0.12	2.0×10^{-11}	5.3×10^{-8}
E3	0.89	0.19	2.0×10^{-8}	2.0×10^{-5}

Figure Captions

Figure 1. Pairwise plot of clustered data for main deep-levels in β-Ga_2O_3. (a,e,i) – distributions of experimental parameters for trap clusters. (b,c,f) and (d,g,h) – represents the same data and shows correlation within measured parameters. These scatter plots demonstrate no correlation of σ_n^m or E_a^m with T_{peak}, which variance is determined with technique limitations. However, σ_n^m strongly depends on E_a^m and this phenomenon will be studied more thoroughly in sections below. (j) – one of the DLTS measurements from the gathered data, which provides 3 of 1242 data entities represented with Arrhenius plot (k) and attributed to E1, E2 and E4 levels.

Figure 2. Configurational diagram. E_d – energy of electron on a defect with Q = Q_d (non-equal to 0 with presence of electron-lattice interaction) and E_k – exited state which is delocalized and since then Q = 0 (small electron-lattice coupling to local mode Q).

Figure 3. Arrhenius plot and extracted parameters as a function of temperature. Fully analytical model (gradient line) with the accounting of temperature dependence of capture cross-section as eq. (5) and simplified model eq. (15) (red line) of temperature dependence of measured E_a^m and σ_n^m. (a) – Fully analytical Arrhenius plot showing different slope values at low and high temperature, (b) and (c) – E_a^m and σ_n^m calculated from Arrhenius plot showing step-like function and (d) – parametric plot of σ_n^m and E_a^m with full and simplified models based on our E2 data (violet crosses) and others groups data (blue symbols).

Figure 4. Collected data on main deep-levels in β-Ga_2O_3 (magnified plot from Fig 1b) and fit with parameters from Table 1.

Figure 5. E_a^m and σ_n^m distributions of main deep-levels in β-Ga_2O_3, based on collected data.

Figure 6. Fitted model of main deep-levels in β-Ga_2O_3 (data from Table 1).

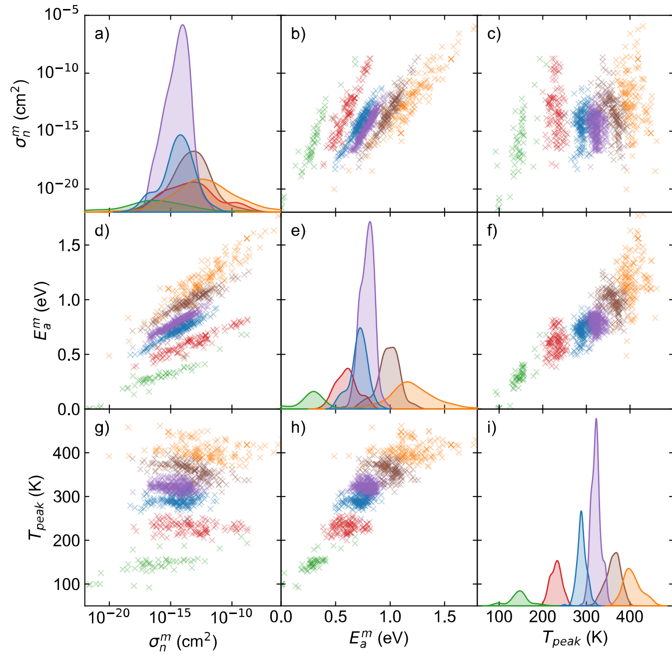

a)
b)
c)
d)
e)
f)
g)
h)
i)
Trap
E2*
E4
E8
E1
E2
E3

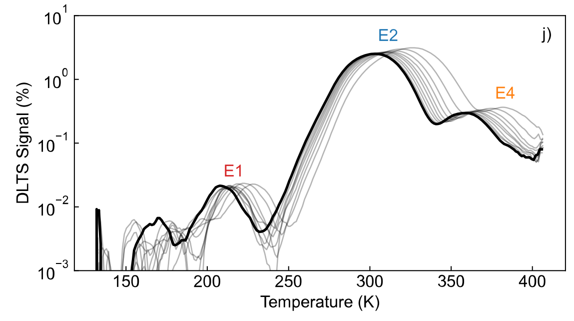

j)
E1
E2
E4
DLTS Signal (%)
Temperature (K)

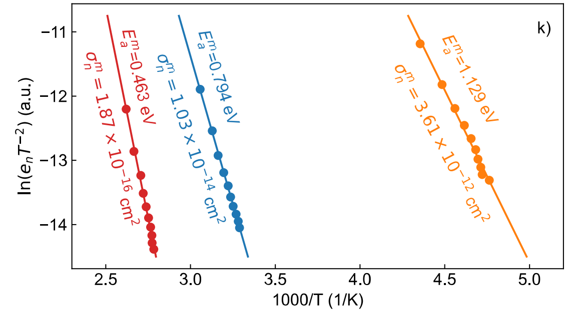

k)
1000/T (1/K)

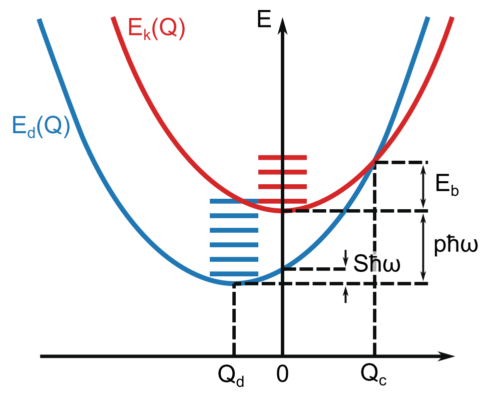
E
$E_k(Q)$
$E_d(Q)$
E_b
$p\hbar\omega$
$S\hbar\omega$
Q_d
0
Q_c

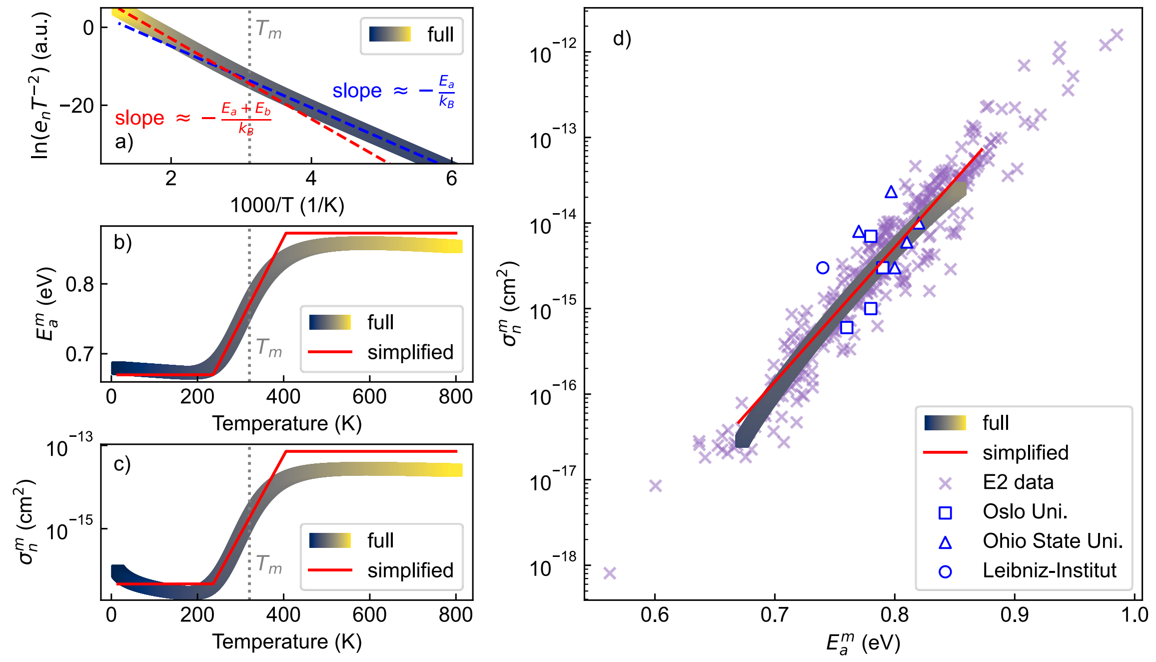

a)
b)
c)
d)
full
simplified
E2 data
Oslo Uni.
Ohio State Uni.
Leibniz-Institut
T_m
slope ≈ $-\frac{E_a}{k_B}$
slope ≈ $-\frac{E_a+E_b}{k_B}$
$\ln(e_n T^{-2})$ (a.u.)
1000/T (1/K)
E_a^m (eV)
Temperature (K)
σ_n^m (cm^2)

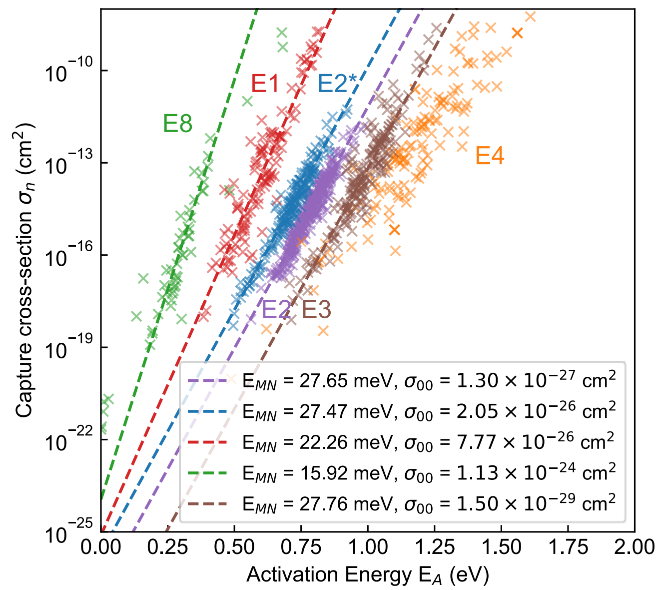

E8
E1
E2*
E4
E2
E3
E_{MN} = 27.65 meV, σ_{00} = 1.30 × 10^{-27} cm^2
E_{MN} = 27.47 meV, σ_{00} = 2.05 × 10^{-26} cm^2
E_{MN} = 22.26 meV, σ_{00} = 7.77 × 10^{-26} cm^2
E_{MN} = 15.92 meV, σ_{00} = 1.13 × 10^{-24} cm^2
E_{MN} = 27.76 meV, σ_{00} = 1.50 × 10^{-29} cm^2
Capture cross-section σ_n (cm^2)
Activation Energy E_A (eV)
10^{-10}
10^{-13}
10^{-16}
10^{-19}
10^{-22}
10^{-25}
0.00
0.25
0.50
0.75
1.00
1.25
1.50
1.75
2.00

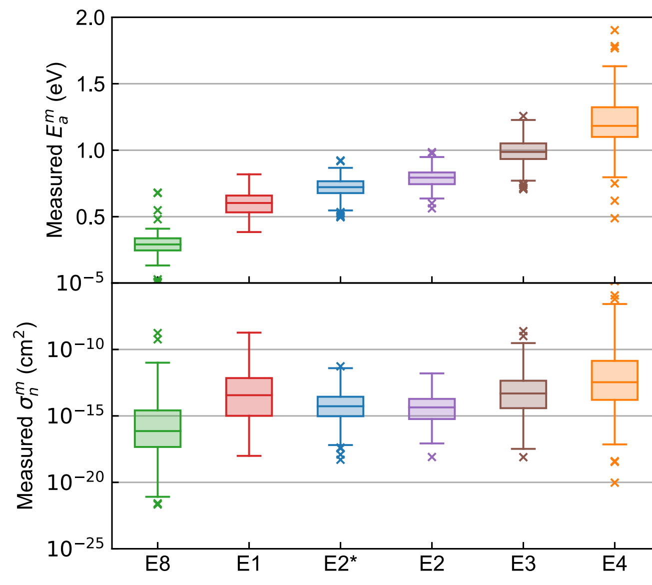

2.0
1.5
1.0
0.5
Measured E_a^m (eV)
10^{-5}
10^{-10}
10^{-15}
10^{-20}
10^{-25}
Measured σ_n^m (cm^2)
E8
E1
E2*
E2
E3
E4

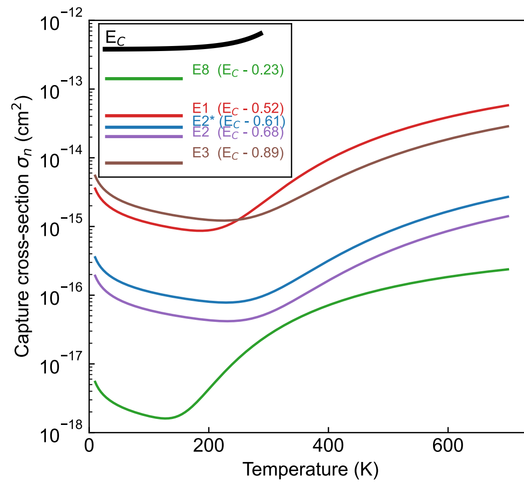

E$_C$
E8 (E$_C$ - 0.23)
E1 (E$_C$ - 0.52)
E2* (E$_C$ - 0.61)
E2 (E$_C$ - 0.68)
E3 (E$_C$ - 0.89)
Capture cross-section σ_n (cm^2)
Temperature (K)